# Drop Camera:
# In Search of the Lost Whaling Fleet

*Grace Cardarelli*
*Myles Riddell*
*Devon Snell*
04/24/15

# Contents

Introduction ..... 3
Abstract ..... 4
Design Considerations ..... 6
Software ..... 10
Experimental Procedures ..... 13
Appendix ..... 23
References: ..... 27

Figure 1: Shows the camera assembly including cameras and fins ..... 7
Figure 2: Shown is the female portion of the two part fins ..... 8
Figure 3: Video cable connected to custom GoPro housing (12V power cable included in final design) [1] ..... 10
Figure 4: Video cable and 12V power cable coming out of custom GoPro housings [1] ..... 10
Figure 5: Front Panel of LabView live video feed from GoPro navigational camera ..... 11
Figure 6: Globalsat USB GPS receiver [2] ..... 12
Figure 7: Front Panel of GPS data conversion ..... 12
Figure 8: Tow tank carriage and tow point marked with red dot ..... 13
Figure 9: Free Body Diagram of Towing System [4] ..... 14
Figure 10: Simplified Free Body Diagram as a Mass-Spring-Damper System ..... 15
Figure 11: Simulink Model of Mass-Damper System (neglecting gain from k) ..... 16
Figure 12: Damping Coefficient as a Relation to Velocity (4' cable length) ..... 16
Figure 13: Damping Coefficient as a Relation to Velocity (6' cable length) ..... 17
Figure 14: Damping Coefficient as a Relation to Velocity (8' cable length) ..... 17
Figure 15: 8-feet cable length, 1.5 knots (x-axis is time [seconds], y-axis is height [feet]) ..... 18
Figure 16: Pressure sensor data converted to height below water surface ..... 19
Figure 17: Depth at 4 feet for all three speeds (two trials each) ..... 19
Figure 18: Depth at 6 feet for all three speeds (two trials each) ..... 20
Figure 19: Depth at 8 feet for all three speeds (two trials each) ..... 22
Figure 20: 2-Fin Design vs. 1 Fin Response Times vs. Speed ..... 24

Table 1: Experimental Time Constants at 4' ..... 20
Table 2: Experimental Time Constants at 6' ..... 21
Table 3: Experimental Time Constants at 8' ..... 22
Table 4: Fin Design Tow Tank Results ..... 23

# Introduction

Almost 150 years ago, whaling ships from California, Hawaii, and New England set sail off the coast of Wainwright, Alaska. All of the 32 ships were suddenly and unexpectedly trapped between ice and shore in a constantly and quickly diminishing stretch of open water with no chance to escape. One ship was hauled across the rugged ice and rowed 90 miles back to shore. The remaining 32 ships were sunk or burned after they were abandoned.

In August 2015, a team of NOAA researchers are traveling back up to this coast of the Arctic Ocean in order to map the shipwrecks on the ocean floor. Previously, researchers have taken side-scan images of the area of interest, but they do not give an accurate depiction of what they are actually seeing, e.g. shadow, trench, oil container, or ship debris. Once the side-scan images present likely or anticipated ship debris, it makes sense for the researches to get actual high quality underwater footage of the area. The depth of the shipwrecks may be up to 150 feet.

A drop camera is used for this purpose—it is towed with a winch cable off the back of an A-frame vessel. In the past, drop cameras have been designed using trial and error based on cost or specific needs for each mission.

The purpose of this project is to research create a cost efficient drop camera that will collect live video footage of the shipwrecks which can be seen by the researchers aboard the vessel. Besides the live footage, two separate cameras will also record everything below and to the sides of the drop camera for complete coverage of the intended area. The software on the laptop aboard the vessel will collect the video footage as well as the drop camera position and distance from the ocean floor.

In order to do this we use a pressure sensor to calculate the depth that the system is under the surface of the water. Using the depth of the drop camera, the length of the cable, and the GPS coordinates of the boat, we are able to precisely locate the items seen by the drop camera. The LabView template that we are using will give us a time stamp along with the corresponding GPS coordinates of the system.

Since most drop camera systems are based on trial and error, the products of this research will assist scientists in the future to utilize these low-cost components and techniques for their research requirements.

# Abstract

Given our constraints and requirements, our final design can be seen in Figure 1. We chose a corrosion resistant, round-bar material for the frame that will also be heavy enough to reduce movement underwater when hovering over a target. From our experiments, we are able to successfully calculate the tow angle of the drop camera, which determines the angle of the navigational camera in front.

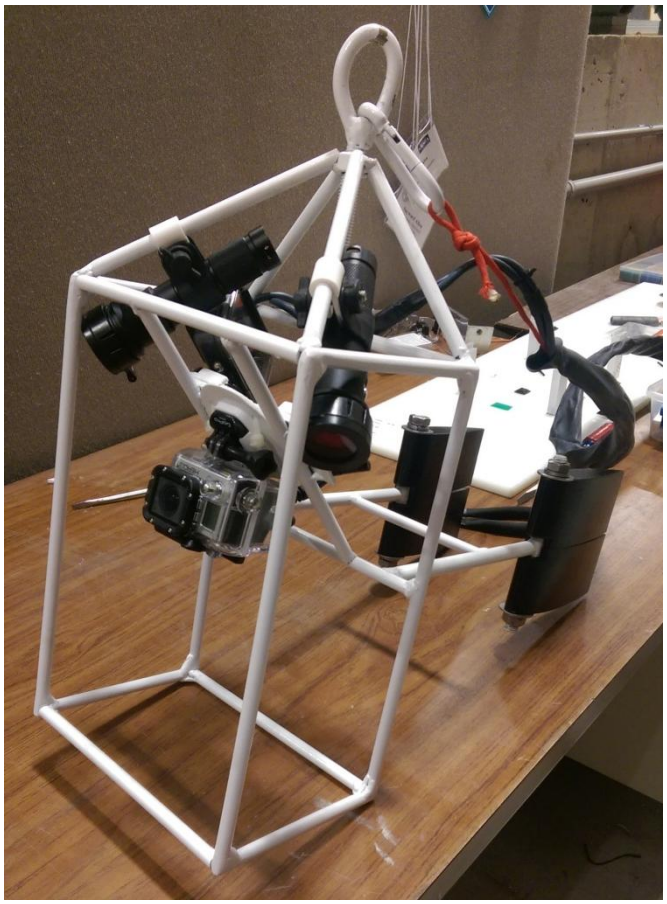

**Figure 1: Final Drop Camera Design**

All three cameras are GoPro because the brand is reliable and they provide the highest quality video for the lowest price. Two cameras point out to the side of the drop camera and down towards the ground. When being towed, the cameras will cover the ocean floor in front of them and out to the side with their impressive 170 degree angle of view. These cameras are for data collection only—a live feed is not necessary, but a power supply may be.

Big Blue dive lights were also chosen for their reliability and quality. They have red lenses to reduce the light attenuation underwater. The two dive lights are mounted in the same direction as the side-facing GoPros to maximize quality of data collection.

A pressure sensor is attached at the bottom of the frame to get an accurate reading of the depth of the drop camera. A Globalsat USB GPS is plugged in to the laptop to read the physical

location of the drop camera. All of this data is consolidated into a customized LabView program that the researchers will operate aboard the vessel.

The LabView program is specifically useful because the researchers can see what the drop camera sees underwater as well as the specific latitude and longitude of the suspected shipwreck.

We accomplished all of the research and construction at $1500, which is well below our $5000 budget restrictions. Our preliminary designs set the stage for the next generation drop camera that will be used for the NOAA research in August of 2015.

## Design Considerations

Major design parameters for the drop camera system were identified which laid out a clear design plan. The frame had to protect all of the instrumentation onboard, as well as being relatively snag-less given the remote environment it will be operated in. Any damage caused to the system would be incredibly expensive and time consuming to repair—therefore, the design must be reliable and all components must be serviceable in the field. Material choice for the frame also plays a significant part given the harsh, cold ocean environment. It must be able to withstand the salinity and also be effective hydro-dynamically when in motion. Most of the components onboard the drop camera generally require batteries to operate, however when in cold water, battery life is greatly impaired. To combat this, a tether system providing a 12V power source from the surface is required. The next criteria addressed were size and weight. Due to the location, the shipping costs are a major part of the overall expenditure, and should be kept as low as possible. The last major point for consideration is the effectiveness of the camera system at the depth and speed of final operation. The camera is to be operated at a depth of between 10ft and 150ft, and at speeds of as slow as ¼ knot and as high as 2 knots for transport to the next drift location. The frame, due to its initial design was capable of maintaining adequate response and tow stability at higher speeds. Given the larger range of operational speeds, the drop camera required additional improvements at lower speeds.

For the purpose of data collection, we chose to locate the navigation camera in the front facing forward with two data collection cameras facing out to the sides. The important part to keep in mind is that the camera system will tip forward due to drag when in motion. Since the system will be towed at some rate during the whole mission, we mounted the side facing cameras such that they will be flat to the horizon when at speeds of 0.5 to 1 knots. Once tow speeds are chosen for the data collection drifts the cameras can be re-adjusted to be at optimal angles.

The frame needed to be large enough to safely contain all of the instrumentation equipment, and prevent snagging on hanging objects or rocks, while remaining small and light enough to ship. The frame can be seen in the figure in the next page at assembly. As shown, the main body is a vertical box, tethered from the top, and designed to keep the instruments high from the bottom where any impacts could occur. Attached to the main body are fin control arms which are welded to the fin pivots. The fins were designed to be removable to reduce the shipping size, and thus the cost. The frame and all external components must be rugged in order to ensure minimal risk of on-site repairs.

When choosing frame material, two main factors had to be considered. First, the entire frame must remain unaffected by the water and more specifically the salinity of the ocean. To combat this issue our frame is made of 316 series Stainless Steel, which is noted for its excellent corrosion resistance. The second main decision that was made regarding frame materials is the cross section. Given the common options of square stock, flat bar, and round bar, the decision was obvious to utilize round bar for several reasons. Round bar will not track sideways due to being caught by flowing currents, and also the wake behind a cylindrical cross section is much

more predictably small than for that of a flat plate or square which may have vortices form behind it. The final size for the drop camera unit is 3/8” SS Round bar for most frame rails, a flat plate for easy mounting of the cameras, and ½” SS Round bar for the fin control arms and pivots.

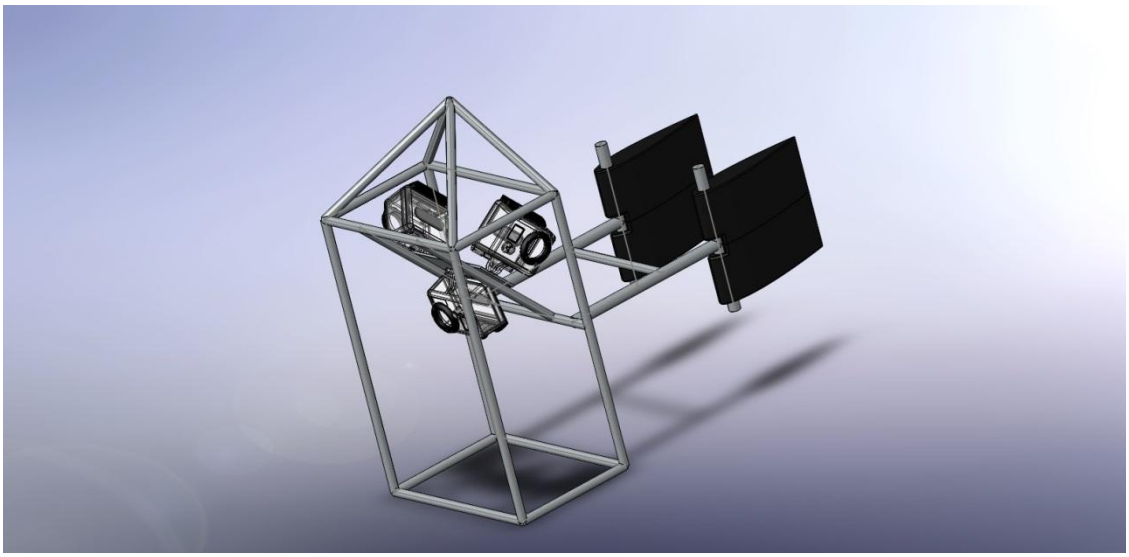

**Figure 2: Shows the camera assembly including cameras and fins**

Fin design and choice was an addition that was made due to data collected in initial testing. During initial tests, the camera system would tow as expected and would track properly at higher speeds, generally greater than 1 knot. This however, being at the higher end of the spectrum, was unsatisfactory. To correct this, two piece modular fins were designed to improve stability at slower speeds. Along with this addition, the response time to directional changes was greatly improved. As shown in the figure on the next page is one of the four total fin parts, the fins are made of two pieces each, each with a mating male/female component to ensure locking and simple assembly. This allowed for the fins to be assembled and adjusted about a central pivot, using minimal hardware and thus, smaller service times. The control arms were sized at 8” in length to provide an adequate moment arm over the pivot of the frame, thus allowing the system to respond to changes in direction, always facing against the direction of flow. To counter the addition of weight of the control arms and pivot mounts, a choice to utilize FDM 3D printing of a hollow PC-ABS plastic gave buoyancy which corrected for the change in tow geometry from the added weight. The choice for the shape of the fins was not a trivial one, given that it would greatly contribute to the overall stability of the system. As shown in the figure on the next page, the shape of the fins is a NACA 0012 Airfoil, which provides no lift due to camber, yet yields a very low drag coefficient, often only about 10% of a cylinder at the same cross section opposing the flow. The fins are about 6 inches long and are the airfoil shape extruded for a total of 6 inches of height.

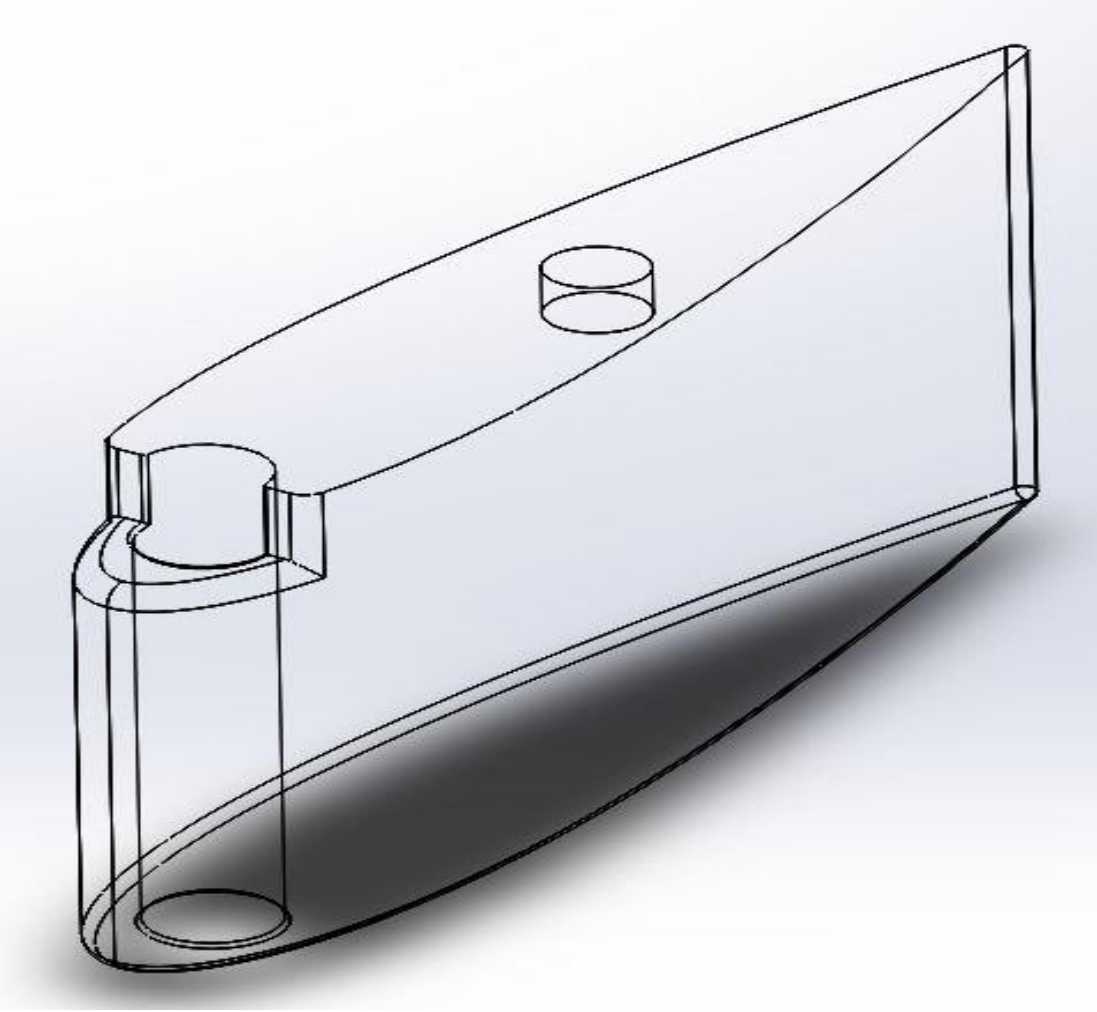

**Figure 3: Shown is the female portion of the two part fins**

Above is one half of a fin assembly, specifically the female receiving side. This, when coupled with the male half can be assembled with only two nuts and washers. The fins were designed to allow a certain degree of adjustment to compensate for any changes in the frame. The roughly +/- 10 degree adjustment allows for corrections to yaw of the frame for a variety of reasons, whether for additional components that increase drag asymmetrically.

The last major design choice made were the components utilized on the frame. The major components are the three camera systems, one tethered to the surface for navigation, and two solely for data collection. The leading camera systems for this application are GoPro cameras. They are effective in very harsh environments, durable, take quality videos, and also are relatively inexpensive. The GoPro's that we chose to use are Hero 3' s, capable of 1080p video capturing, and also capable of live feedback in 720p back to the surface through an aftermarket tether. Our navigation camera is the only system which required live feedback, though the other two would benefit from such. The tether system used for live feedback is produced by a company called EyeOfMine. The camera waterproof housing is capable of operation in up to 200ft underwater. The housing also has ports which allow cables to run 720p live footage and

also 12V charging, giving a virtually limitless operation time before retrieval of the system. The two data collection cameras do not currently have such a tether, thus the operation duration has to be kept within the limitations of the battery life, which is not much more than an hour in extreme cold waters. For uninterrupted operation, tethers for all three cameras would allow for data collection drifts to be performed much longer without service, only limited by the memory capabilities of the cards in the cameras. Though not necessary for the initial mission in August, the cameras are supported for darker ocean conditions by two 900 lumen dive lights. These lights, when equipped with filters will improve video quality at further depths. Custom adaptor brackets were designed and 3D plastic printed to attach to the frame while retaining adjustability of beam direction.

In summary, the drop camera system was designed to fulfill certain criteria. The system is light and compact thus making it cheap and easy to ship to northern Alaska. The robustness of the frame will allow worry free operation, with little risk of damage to the instrumentation. The entire system is waterproof up to depths that far exceed the mission parameters, also highly corrosion resistant. Throughout all phases of operation, through various depths and different towing speeds, the camera will remain stable and will respond to directional changes as input from the tow vessel. The live feed camera will provide navigation information to the surface while the two side cameras record high quality video for analysis upon retrieval of the system.

# Software

The software was consolidated into a simple LabView interface. First, the live video feed comes out of the custom GoPro waterproof housings as seen in the close-up in Figure 4and connect to a USB-RCA adapter. Figure 5shows the video cable as well as the 12V power cable coming out of the GoPro.


**Figure 4: Video cable connected to custom GoPro housing (12V power cable included in final design) [1]**

**Figure 5: Video cable and 12V power cable coming out of custom GoPro housings [1]**

The live video can be seen in the LabView Front Panel in Figure 6. The user is initially prompted to choose a video source when running the program and the video will display in the dark area shown in the figure below.

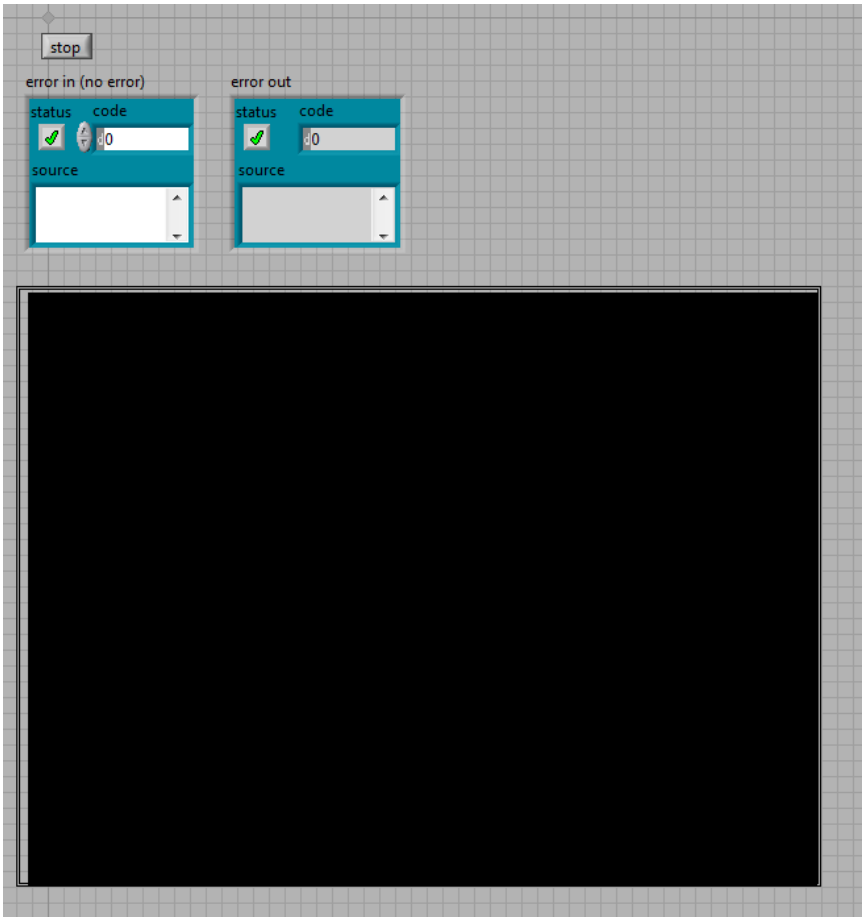


**Figure 6: Front Panel of LabView live video feed from GoPro navigational camera**

The Globalsat USB GPS seen in Figure 7 below also connects to the laptop on board the vessel. When connected, the latitude and longitude is graphed in the LabView Front Panel (Figure 8), and the speed of the vessel is recorded. The researchers will match the video with the GPS coordinates to visualize the location of the shipwrecks.


**Figure 7: Globalsat USB GPS receiver [2]**

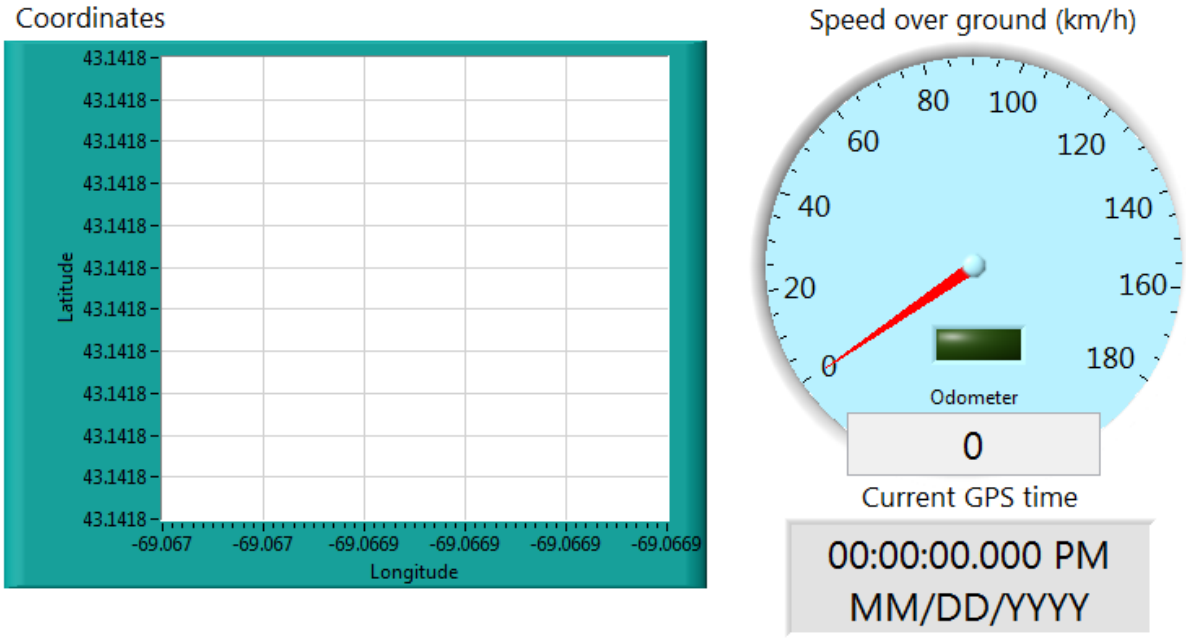


**Figure 8: Front Panel of GPS data conversion**

## Experimental Procedure 1—Depth Analysis

### Setup:

All experiments were performed in the Chase Ocean Engineering lab in the wave/tow tank. It is 8 feet deep and 12 feet wide and includes observation windows below the surface of the water. The drop camera system consists of 3 GoPro cameras with deep water housings, a HOBO pressure sensor, a stainless steel frame, and 50 feet of video and power cables that are all towed by a stainless steel cable. A thinner cable was chosen in order to increase weight ratio between the drop camera and the cable. This prevents the cable from excessive slacking while being towed. A picture of the experimental setup can be seen in Figure 9 below.

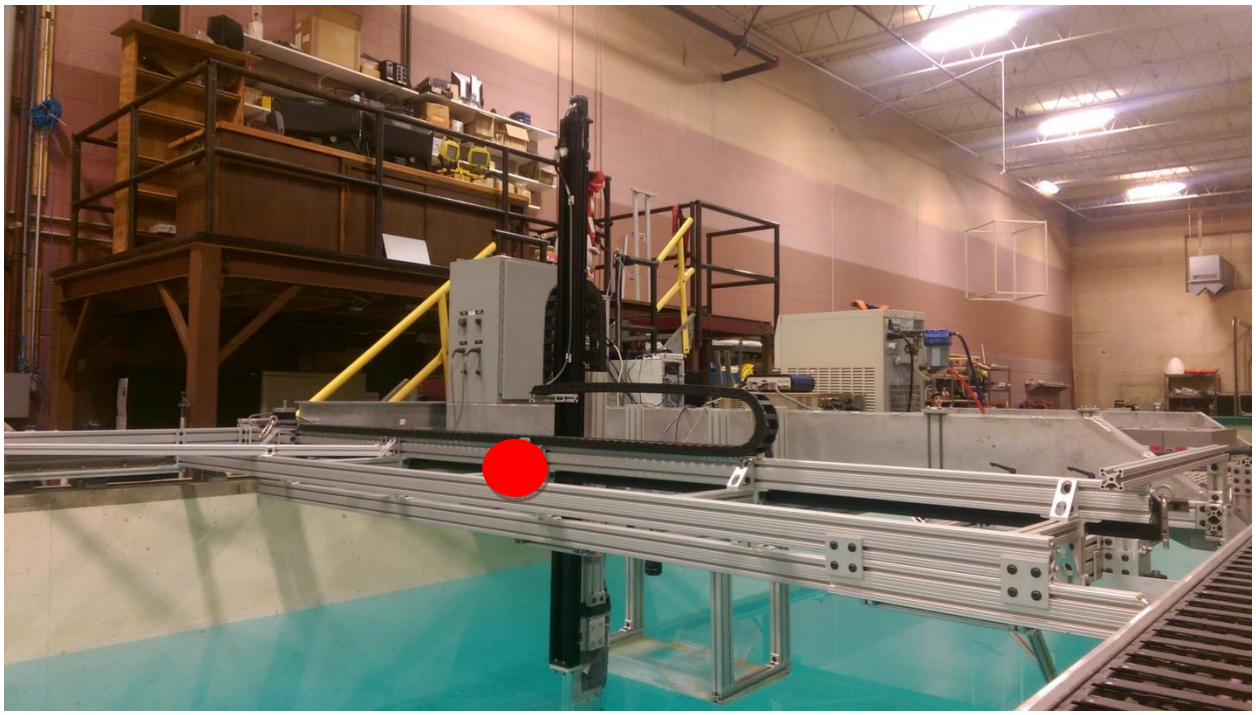

**Figure 9: Tow tank carriage and tow point marked with red dot**

### Theoretical Response:

The system shown in Figure 10 is an illustration of the drop camera being towed with all of the corresponding forces acting on it. In the bottom left corner of the figure, there is a free body diagram of the summed forces in the x and y directions acting on the drop camera.

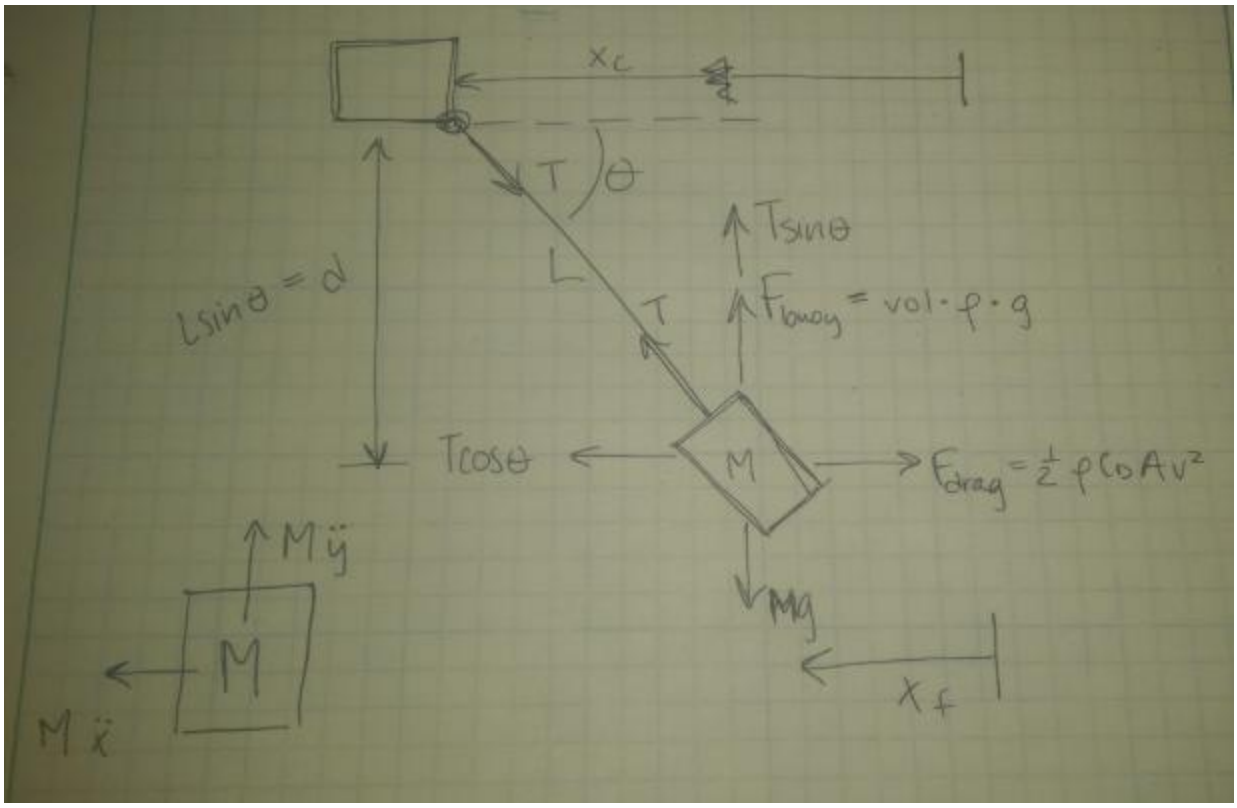


**Figure 10: Free Body Diagram of Towing System [3]**

A mathematical model for both the x and y directions are shown in Equations 1 and 2 respectively.

$$\boldsymbol{m_f \ddot{x}_f = T\cos\theta - \frac{1}{2}\rho C_d (\dot{x_f})^2} \quad (1)$$

$$T = tension\ in\ tow\ cable$$

$$x_f = total\ distance\ traveled$$

$$C_D = coefficient\ of\ drag$$

$$\boldsymbol{m_f \ddot{y}_f = T\sin\theta - (w - B)} \quad (2)$$

$$w = m_f g, \quad B = (vol)\rho g$$

$$y_f = vertical\ change\ in\ height\ of\ drop\ camera$$

These equations along with Equations 3 and 4 relate the angle (θ) of the towline to the horizontal line of water.

$$\boldsymbol{x_f = x_c - l\cos\theta} \quad (3)$$

$$x_c = distance\ from\ drop\ camera\ to\ tow\ point$$

$$l = length\ of\ tow\ cable$$

$$y_f = l(1 - sin\theta) \quad (4)$$

The equations above are derived assuming that the towline is taut. Other assumptions that we made in an attempt to make the math simpler were that the tension (T) and angle (θ) were linear during acceleration of the tow carriage. Another issue we ran into was linearizing the horizontal position ($x_f$)—this issue along with our previous assumptions of the theoretical model created a skewed amplitude. We credit this high amplitude to the multiple assumptions that we made in order to simplify our system. To potentially solve this issue in the future, we plan on attaching a potentiometer onto the tow point of the cable to measure angular displacement. With this data, we could reduce our unknown variables.

Figure 11 below shows the drop camera modeled as amass-spring-damper system in the vertical direction—we are only considering the vertical direction because we are only looking for the change in height of the drop camera. We modeled it this way because we are able to find equivalent values for the damping coefficient and spring constant.

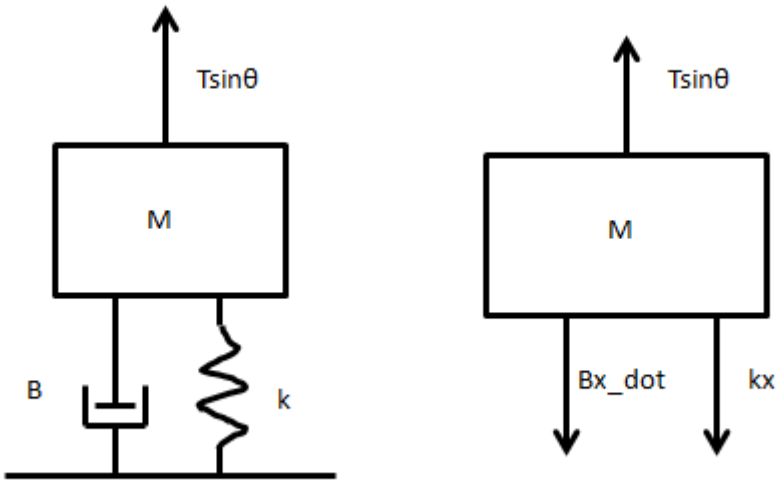


**Figure 11: Simplified Free Body Diagram as a Mass-Spring-Damper System**

From the free body diagram above, we were able to derive a mathematical model of the system as seen in Equation 5.

$$M\ddot{x} + B\dot{x} + kx = Tsin\theta \quad (5)$$

The spring constant (k) represents the stiffness of the drop camera. Since it is made of stainless steel, the stiffness of the frame is so high that the value of k is negligible. Compared to the total displacement of the drop camera in the water, the distance that the frame is displaced is much greater than the distance displaced by the stiffness. The mass (M) of our system is the mass of the drop camera frame that holds the cameras.

The damping coefficient (B) was estimated based on the trends seen in our experimental data [3]. We used Simulink to model our system as shown in Figure 12.

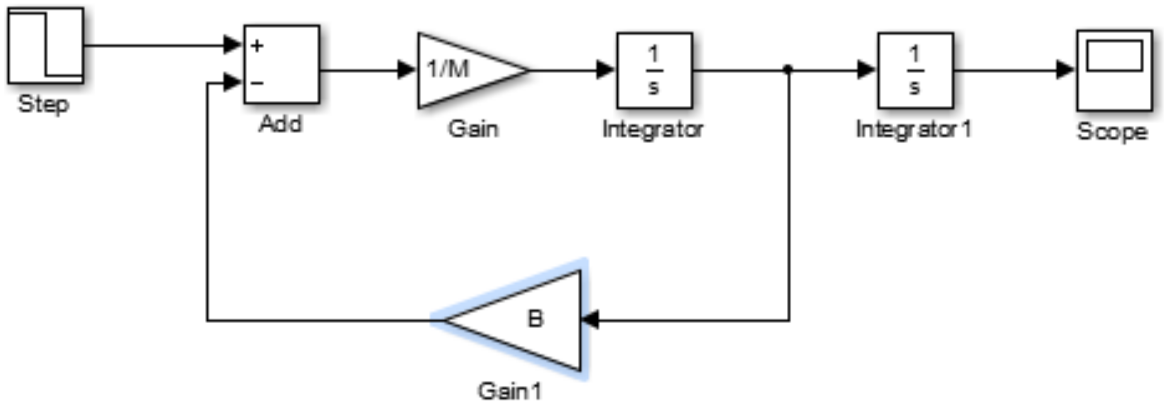


**Figure 12: Simulink Model of Mass-Damper System (neglecting gain from k)**

Based on the steady-state time for each trial (at each speed and cable length), we changed the step response time as well as the damping coefficient (B). We changed the value of B to agree with the height change of our experimental data—then we were able to find the trend of the damping coefficient for each length of cable. Figures 13-15 show the damping coefficients versus the velocity of the drop through the water. We fit a second order function to each of the cable lengths, which can be seen below their respective figures in Equations 6-8.

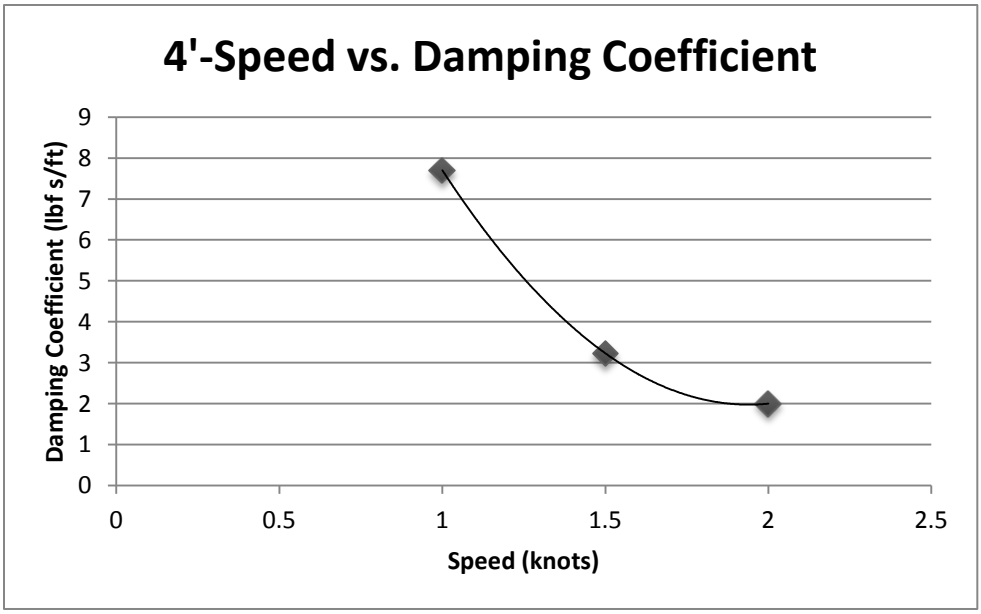


**Figure 13: Damping Coefficient as a Relation to Velocity (4' cable length)**

$$B_{4-feet} = 0.648v^2 - 25.14v + 26.36 \quad (6)$$

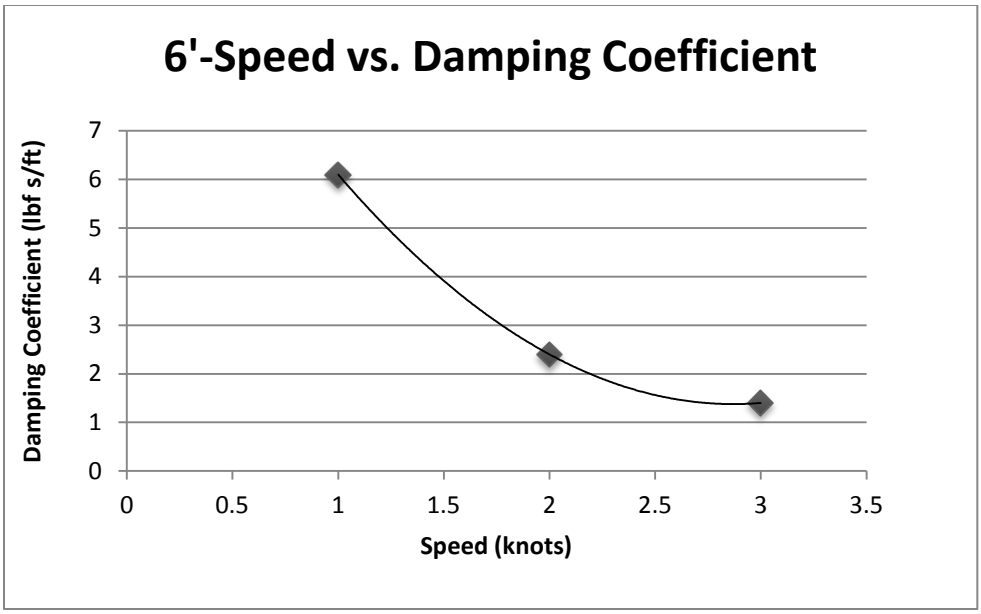


**Figure 14: Damping Coefficient as a Relation to Velocity (6' cable length)**

$$B_{6-feet} = 1.35v^2 - 7.75v + 12.5 \quad (7)$$

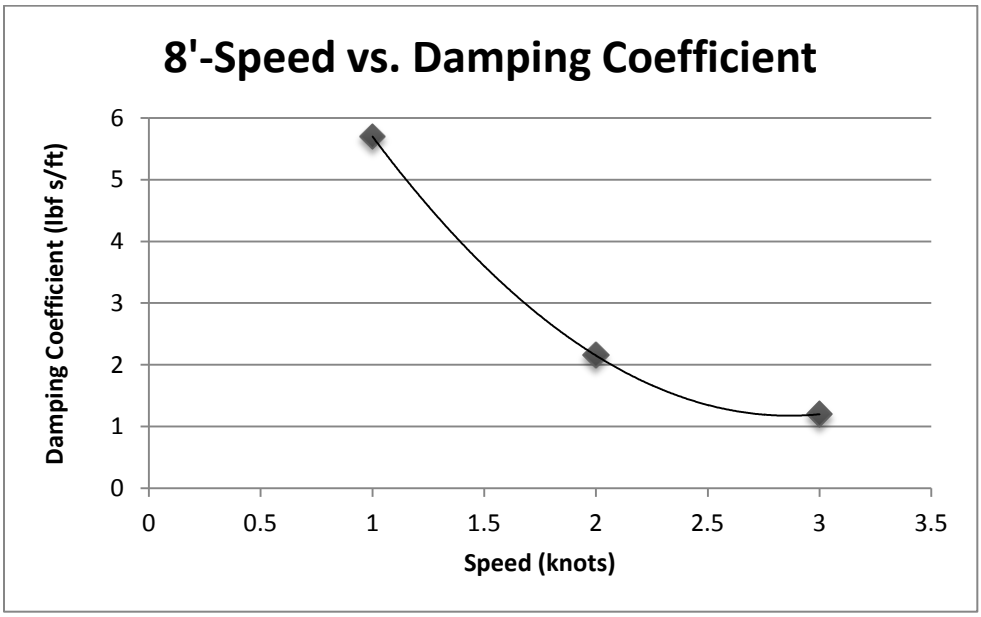


**Figure 15: Damping Coefficient as a Relation to Velocity (8' cable length)**

$$B_{8-feet} = 1.3v^2 - 7.45v + 11.85 \quad (8)$$

The figure below is the Simulink theoretical response of our equivalent mass-damper system. Based on this model, we are unable to completely express the height response because

our system only considers the y displacement of the drop camera. We expect that with a fully-defined model the height response would be smoother like in our experimental data. The figure below shows the response of an 8-foot cable length with a steady-state height of 1.2 feet after the drop camera reached its steady-state speed.

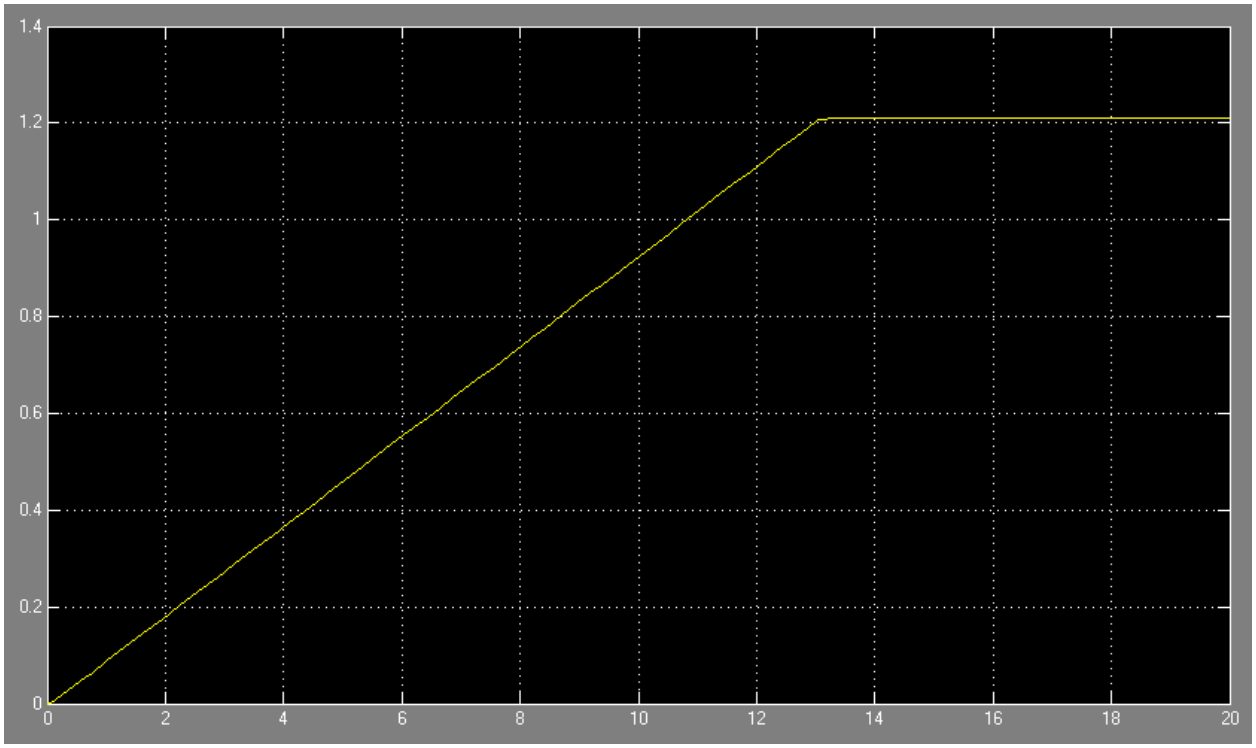


**Figure 16: 8-feet cable length, 1.5 knots (x-axis is time [seconds], y-axis is height [feet])**

## Experimental Data:

Our experimental data was collected from a waterproof HOBO pressure sensor that reads absolute pressure. We converted all of the pressure data to distance below the surface of the water as seen in Figure 17. At height 0, the drop camera has not touched the water yet. Just after 2000 seconds, we calibrated the pressure sensor to make sure it was reading the right height at the bottom of the tank (see Matlab section of Appendix). Just before 4000 seconds, we began our testing with an 8 foot cable and a velocity of 1 knot. The first two jumps in height are from the first two trials. The next two trials at 1.5 knots have a significantly higher height. After the set of trials at 2 knots, we pulled it back up to the surface to adjust the length of the cable. At 5000 and 6000 seconds, the cable length was changed to 6 feet and 4 feet respectively.

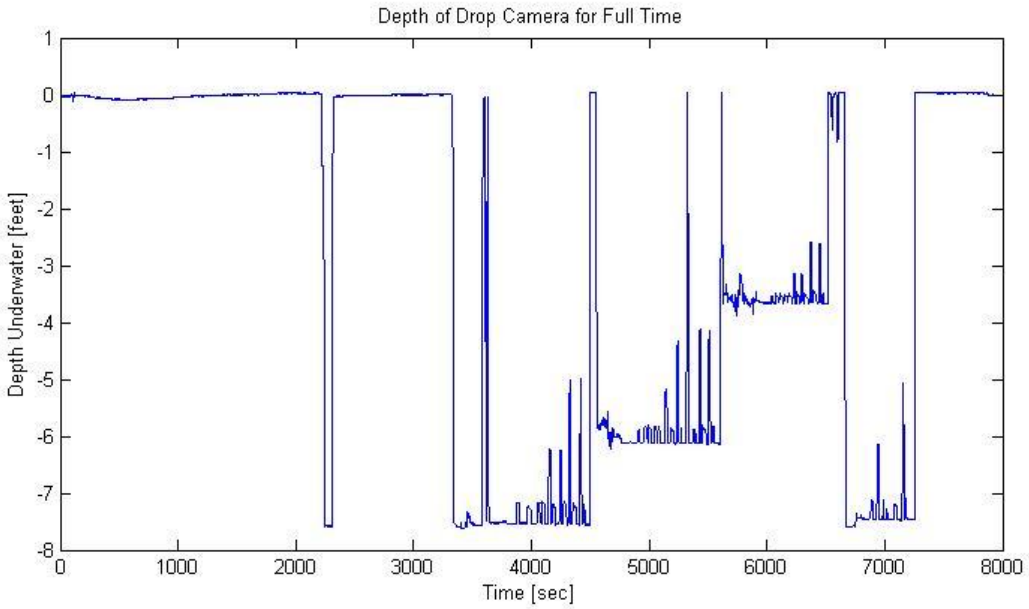


**Figure 17: Pressure sensor data converted to height below water surface**

The experimental responses of height versus time for each cable length can be seen in the following figures. Since the system is over damped and the stiffness (*k*) is negligible, we can find the time constant for each trial run.

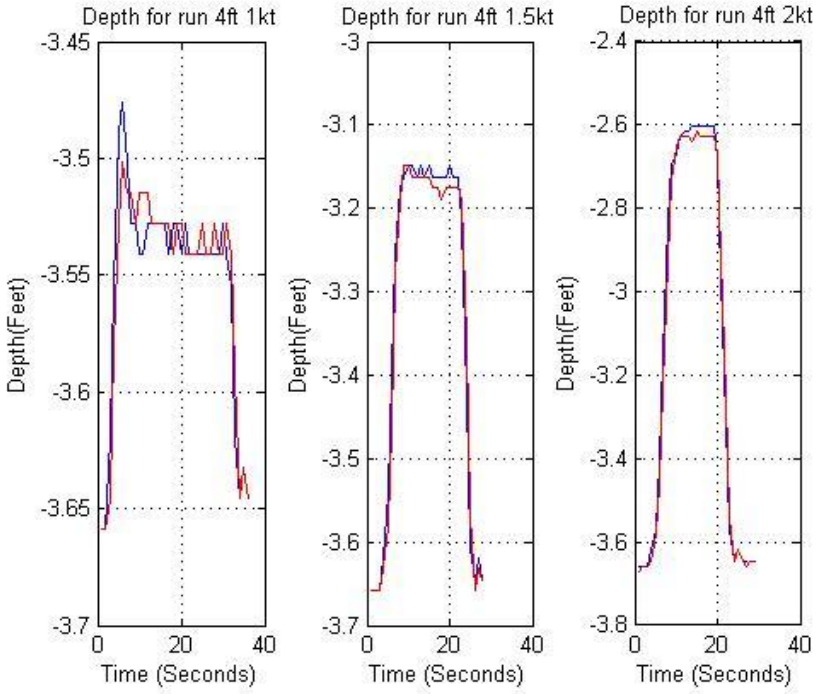


**Figure 18: Depth at 4 feet for all three speeds (two trials each)**

The first run at 4 feet and 1 knot can be seen in the first frame of Figure 18. As soon as the drop camera began to tow, the frame flipped over and the pressure sensor was vertically

displaced. This is shown by the jump in data at the beginning of the trial. The response appears to be under damped according to that data, but the next two trials are a better representation of the drop camera movement.

Table 1 shows the time constants for each of the runs using the 63.2% method. As the drop camera is being towed faster, the height change also increases and it takes longer for it to reach a steady height. This is why the time constant for 2 knots is higher than the slower velocities.

**Table 1: Experimental Time Constants at 4'**

| Trial Run for 4 Feet [knot] | Height at Time Constant [feet] | Time Constant [sec] |
|---|---|---|
| 1 | -3.576 | 2 |
| 1.5 | -3.345 | 3 |
| 2 | -3.007 | 5 |

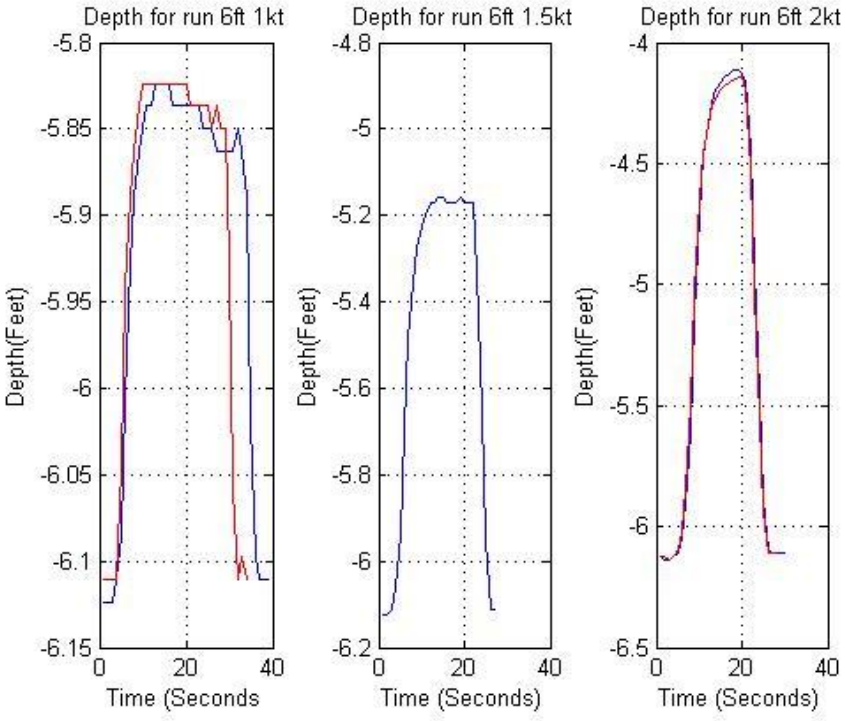


**Figure 19: Depth at 6 feet for all three speeds (two trials each)**

In the first frame of Figure 19, we noticed that there were still oscillations at the steady-state height. The height change during the 1 knot tow was slow which made the drop camera vibrate more—the ratio of drag force to tow force at steady-state height increases as the speed

increases. The drop camera "feels" more force from the water moving around it. Equation 9 shows how the squared velocity is directly proportional to the ratio mentioned above.

$$\frac{F_{drag}}{F_{tow}} = \frac{\frac{1}{2}\rho c_D A v^2}{Macos\theta} \propto v^2 \tag{9}$$

Since the tow tank allowed us limited space, we were unable to get a good segment of steady-state height data.

Table 2 shows the time constants for each of the trials with a 6 foot cable. We saw the same trend as with the 4 foot cable: the time constant increased as the speed increased because the height of the drop camera increased with increasing height.

**Table 2: Experimental Time Constants at 6'**

| **Trial Run for 6 Feet [knot]** | **Height at Time Constant [feet]** | Time Constant [sec] |
|---|---|---|
| 1 | -5.978 | 5 |
| 1.5 | -5.522 | 6 |
| 2 | -4.854 | 9 |

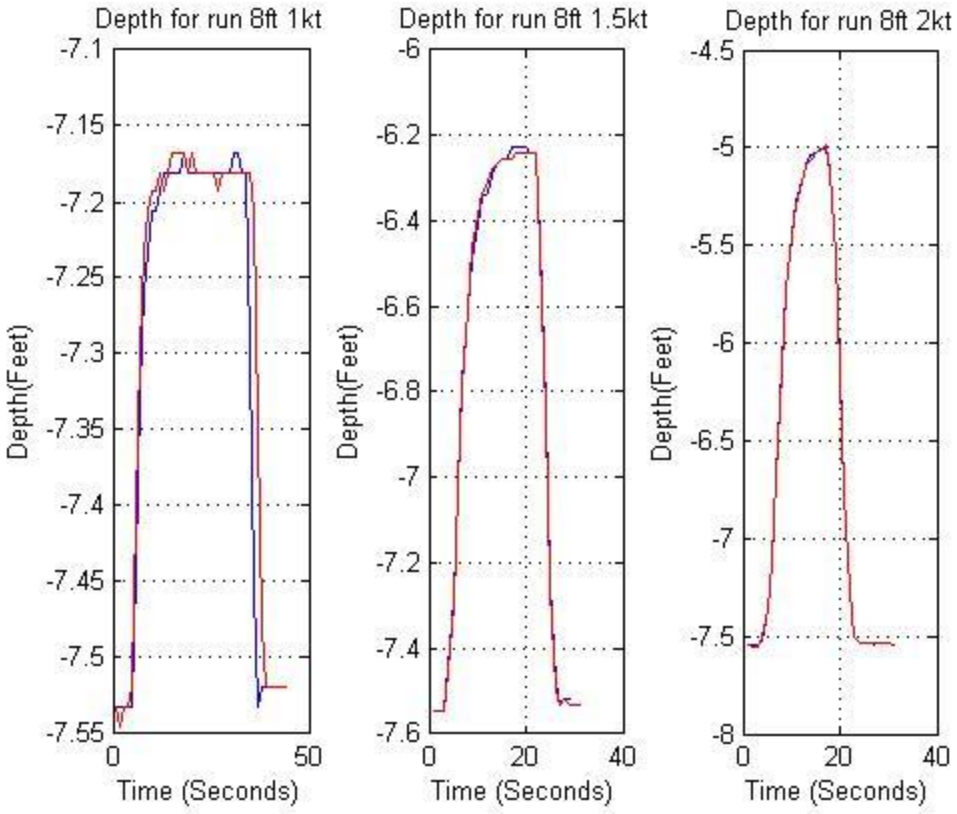


**Figure 20: Depth at 8 feet for all three speeds (two trials each)**

Figure 20 shows the height change at a cable length of 8 feet. As seen in the second and third frames, the drop camera barely even reached its steady-state height. For this reason, the 63.2% method is not going to be as accurate as for the 4 foot and 6 foot trials. Regardless, we still experienced an increase in time constants. Due to the low sensitivity of the HOBO pressure sensor, we were not able to get a more accurate time constant—with a higher sensitivity, the time constant at 1 and 1.5 knots would show a similar trend as seen in Tables 2and 3.

**Table 3: Experimental Time Constants at 8'**

| Trial Run for 8 Feet [knot] | Height at Time Constant [feet] | Time Constant [sec] |
|---|---|---|
| 1 | -7.310 | 6 |
| 1.5 | -6.720 | 6 |
| 2 | -5.934 | 7 |

## Experimental Procedure 2—Re-Design Testing

### Overview:

The main redesign of the drop camera cage was to correct for the undesired rotation of the cage at slower speeds. The earlier design of the drop camera cage performed well under faster speeds but had poor tow stability during slower speeds. In order to correct this, fins were designed (as mentioned above) in order to assist the cage perform correct rotation depending on the tow vessel's direction. The full body test with the new design would test the effectiveness of a 1-fin design compared to a 2-fin model.

The procedure set up would run the tow tank at low speeds (0.25kt, 0.5kt, 0.75kt, and 1kt) in order to address the initial design flaw. The drop camera cage was set to an 8ft, which is the deepest towable point in the tow tank. The procedure included setting up a 'runway' for the tow tank carriage in order to allow for the drop camera cage to get in its fully settled position at the tested speed. When the tow tank carriage approached the end of the runway, the velocity of the carriage would immediately change to the opposite direction (returning to its initial position). At this point a timer was started to test when the drop camera cage returned to a stable position facing in the opposite direction (180 degree change). The determination of this was done using the live feed camera to determine a stable position of the cage.

**Table 4: Fin Design Tow Tank Results**

| | Two Fin | One Fin |
|---|---|---|
| speed [kt] | lapse time [s] | lapse time [s] |
| 0.25 | 13.3 | 14.6 |
| 0.25 | 13.2 | 15.3 |
| 0.25 | 13.5 | 15.7 |
| 0.5 | 8.8 | 9 |
| 0.5 | 8.2 | 9.4 |
| 0.5 | 7.4 | 8.9 |
| 0.75 | 5.5 | 6.8 |
| 0.75 | 5.1 | 6.6 |
| 0.75 | 4.8 | 7.5 |
| 1 | 5.2 | 6.1 |
| 1 | 6.2 | 6.9 |
| 1 | 6.5 | 7 |

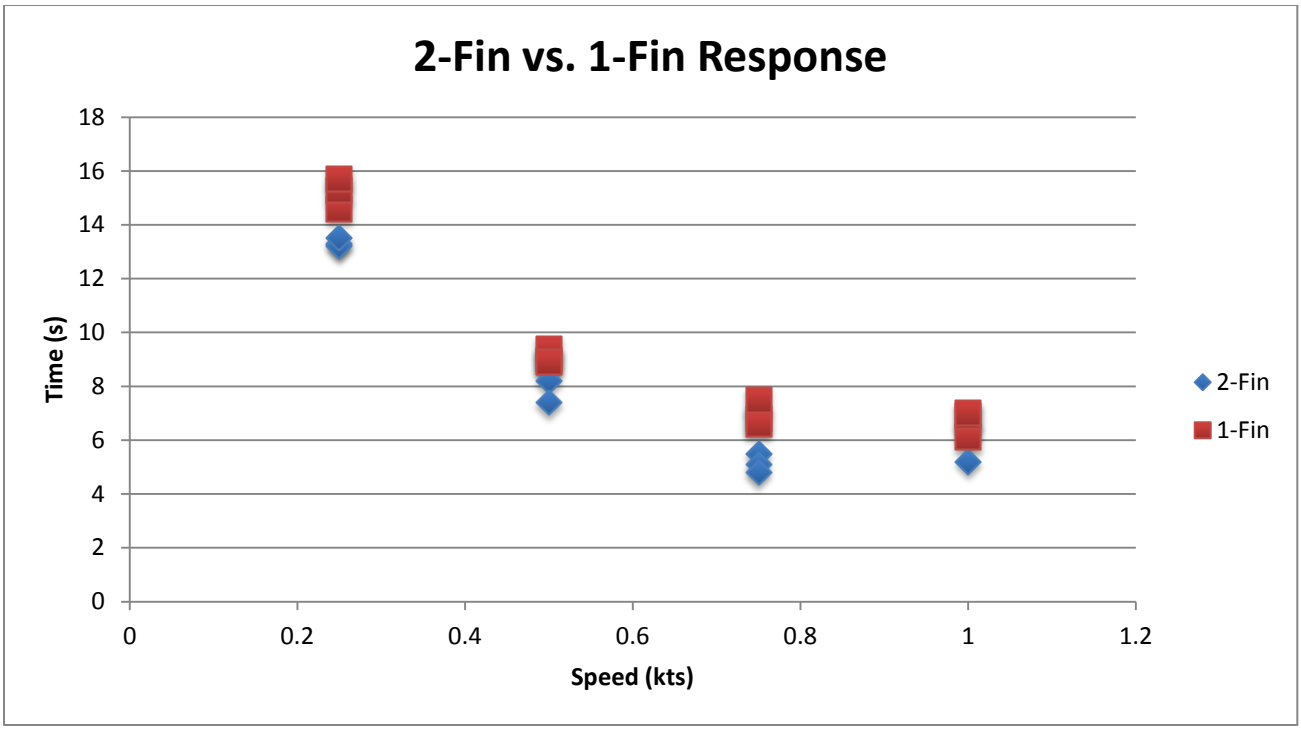


**Figure 21: 2-Fin Design vs. 1 Fin Response Times vs. Speed**

Table 4 and Figure 21 above show the results of the fin direction change test. As seen in the data results, the 2-fin results showed a faster response time to the direction change. The results do only show a slightly faster result in response time in the range .5-1 second. The 2-fin design was chosen not only due to the faster response but also with the 2-fin did not require most adjustment in order for the cage to tow straight. With the 1-fin design, the fins needed to be adjusted to in order to keep the cage at the desired position. The 2-fin design clearly showed more tow stability.

In addition to determining how to correct for the rotation of the drop camera cage, the fin design test also helped determine maximum lost data recording time due to rotation. Although the mission states that the towing vessel will go in straight tow directions in an array in order to gather a rough image of the surface below, the response time will allow the operator how long to overshoot the desired area. The desired tow speed, given as a specification was 1knot but assuming non-ideal situations, the results above show that a direction change of 13 seconds will be more than safe estimate of how much overshoot the vessel can do.

## Design Recommendations

For the August 2015 mission, we have several recommendations in order to complete the desired tasks. The main recommendation is that all cameras be tethered to the tow vessel. Although all cameras don't need to be sent up as live feed the cold water temperatures drastically reduce the battery life of the cameras. Thus for the expedition in August we recommend the eye of mine camera case so the expedition can leave the drop camera cage with the cameras in the water without fear of battery lose. The alternate would be having spare batteries onboard but that is much more inefficient than leaving having a guarantee of power sent to the camera. Another advantage to the power tether being sent down is that crew can see from the observation cameras as well which would allow them to make adjustments as needed without uploading the recording data to a computer.

Another recommendation we will make is to use a more durable and tested pressure sensor. The self-made pressure sensor was an unreliable option and with the remote location of the operation a more durable pressure sensor will prove worthwhile. Although if the depth of drop camera cage can safely be determined by the amount of cable released and be outside the danger zone of any debris then a pressure sensor may not be exactly required. In this case the live feed camera should be angled down in order to monitor the ground activity at a closer distance in order to ensure the safety of the cage and cameras.

The last recommendation we make is to use the lens filters of the camera along with more dive lights. For general testing we only used a limited amount of dive lights but to ensure high quality images and data we recommend use more dive lights along with the filters given to improve image quality. The experiments we performed showed high quality and reliable images but due to the unknown conditions of the wreck locations, extra dive lights should help ensure the quality of the data collected.

## Conclusion

Through the various testing performed throughout the year, the goals set before the year have been met for the drop camera team. The drop camera cage goals were to be reliable, low cost technologies, easy to ship, and easily deployed from the A-frame. The main project goal that was analyzed is the reliability of the frame. The frame was designed with stainless steel for long term use in the ocean while also choosing a proven camera system (GoPro) that can be relied on during the expedition. The self-made pressure sensor as mentioned above did not prove reliable, due to its failure with the power supply. The camera cases, which are recommended from the EyeofMine camera case company, are also recommended to provide a reliable power source to the camera. Also the live feed of the camera can go to multiple outputs, which allow for an accidental malfunction of the LabView software. The design also allowed for easily replaceable parts such as the dive lights, the camera system, and the programs used have the ability to be replaced or fixed on sight so the crew can correct any issues that may arise.

The overall cost of materials of the project is roughly 1500 dollars with all the steel material, cameras, dive lights, wire, etc. This makes the project affordable for the expedition allowing other costs to take more of the budget compared to the camera system itself. The camera system fully assembled can easily fit in a 2ftx2ftx2ft box that would include padding. The other option for the mission team is to disassembly the pieces in order to ship the components conveniently. The towing system is also clipped onto the frame for easy towing off of the vessel, which allows the crew to easily get to the desired pieces of the camera. Through towing testing throughout the year along with testing the individual pieces, the drop camera system met its years goals effectively and through this experience have provided recommendations to aid the crew on its mission to Alaska.

# Appendix

**References:**

[1] http://www.eyeofmineactioncameras.com/GoPro_Hero3_SMALLER_Underwater_ Wired_
[2] http://www.thegpsstore.com/USGlobalSat-BU353-S4-USB-GPS-Receiver-P3219.aspx
[3] Discussions with Professor Swift
[4]https://engineering.purdue.edu/~ce573/Documents/Structural%20damping%20values_JDStevenson.pdf
[5] SolidWorks 2010: Concord, MA: SolidWorks, 2010. Print.
[6] Discussions with Professor Thein
[7] HOBO Pressure sensor: http://www.onsetcomp.com/waterLevelVsCompetition

**Matlab Code:**

```
%% Devon Snell
%  Myles Riddell
%  Grace Cardarelli

clc
clear all
close all

t=1:7915';
t=t';
d=load('P1.txt');

d1=d(:,1)/(9.81)*(3.32084);
d1=(d1(:,1)-34.08)*-1;
% plot(t, d1)
% title('Depth of Drop Camera for Full Time')
% xlabel('Time [sec]')
% ylabel('Depth Underwater [feet]')

%% Seperating trials
r81(1:40,1)=d1(3864:3903,1);
x81(1:40,1)=sqrt(64-r81.^2);
t81=1:40;

% figure
% subplot(1,3,1)
% plot(t81,x81)
% title('x Displacement of 8-foot Cord at 1 knot')
% xlabel('Time [sec]')
% ylabel('Displacement [ft]')
%
r815(1:29,1)=d1(4140:4168,1);
t815=1:29;
% x815(1:29,1)=sqrt(64-r815.^2);
% subplot(1,3,2)
% plot(t815,x815)
```

```
% title('x Displacement of 8-ft Cord at 1.5 knots')
% xlabel('Time [sec]')
% ylabel('Displacement [ft]')
%
r82(1:27,1)=d1(4314:4340,1);
t82=1:27;
% x82(1:27,1)=sqrt(64-r82.^2);
% subplot(1,3,3)
% plot(t82,x82)
% title('x Displacement of 8-ft Cord at 2 knots')
% xlabel('Time [sec]')
% ylabel('Displacement [ft]')
%

r61(1:39,1)=d1(4951:4989,1);
t61=1:39;
% x61(1:39,1)=sqrt(6.14^2-r61.^2);
% figure
% subplot(1,3,1)
% plot(t61,x61)
% title('x Displacement of 6-ft Cord at 1 knots')
% xlabel('Time [sec]')
% ylabel('Displacement [ft]')
%
r615(1:27,1)=d1(5129:5155,1);
t615=1:27;
% x615(1:27,1)=sqrt(6.14^2-r615.^2);
% subplot(1,3,2)
% plot(t615,x615)
% title('x Displacement of 6-ft Cord at 1.5 knots')
% xlabel('Time [sec]')
% ylabel('Displacement [ft]')
%
r62(1:30,1)=d1(5415:5444,1);
t62=1:30;
% x62(1:30,1)=sqrt(6.14^2-r62.^2);
% subplot(1,3,3)
% plot(t62,x62)
% title('x Displacement of 6-ft Cord at 2 knots')
% xlabel('Time [sec]')
% ylabel('Displacement [ft]')


r41(1:36,1)=d1(6067:6102,1);
t41=1:36;
% x41(1:36,1)=sqrt(16^2-r41.^2);
% figure
% subplot(1,3,1)
% plot(t41,x41)
% title('x Displacement of 4-ft Cord at 1 knot')
% xlabel('Time [sec]')
% ylabel('Displacement [ft]')

r415(1:28,1)=d1(6216:6243,1);
t415=1:28;
% x415(1:28,1)=sqrt(16^2-r415.^2);
```

```
% subplot(1,3,2)
% % plot(t415,x415)
% title('x Displacement of 4-ft Cord at 1.5 knots')
% xlabel('Time [sec]')
% ylabel('Displacement [ft]')

r42(1:27,1)=d1(6357:6383,1);
t42=1:27;
% x42(1:27,1)=sqrt(16^2-r42.^2);
% subplot(1,3,3)
% plot(t42,x42)
% title('x Displacement of 4-ft Cord at 2 knots')
% xlabel('Time [sec]')
% ylabel('Displacement [ft]')

r81a(1:44,1)=d1(4041:4084,1);
t81a=1:44;
r815a(1:31,1)=d1(4233:4263,1);
t815a=1:31;
r82a(1:31,1)=d1(4406:4436,1);
t82a=1:31;

r61a(1:34,1)=d1(5034:5067,1);
t61a=1:34;
r62a(1:28,1)=d1(5496:5523,1);
t62a=1:28;

r41a(1:36,1)=d1(6141:6176,1);
t41a=1:36;
r415a(1:28,1)=d1(6284:6311,1);
t415a=1:28;
r42a(1:29,1)=d1(6436:6464,1);
t42a=1:29;


%% Data Plot
figure(1)
plot(t,d1(:,1));
title('Depth for full time (7915 Secs)')
xlabel('Time (Seconds)')
ylabel('Depth(Feet)')
grid on

figure(2)
subplot(1,3,1)
plot(t81,r81,'b',t81a,r81a,'r');
title('Depth for run 8ft 1kt')
xlabel('Time (Seconds)')
ylabel('Depth(Feet)')
grid on

subplot(1,3,2)
plot(t815,r815,'b',t815a,r815a,'r');
title('Depth for run 8ft 1.5kt')
xlabel('Time (Seconds)')
```

```
ylabel('Depth(Feet)')
grid on

subplot(1,3,3)
plot(t82,r82,'b',t82a,r82a,'r');
title('Depth for run 8ft 2kt')
xlabel('Time (Seconds)')
ylabel('Depth(Feet)')
grid on

figure(3)
subplot(1,3,1)
plot(t61,r61,'b',t61a,r61a,'r');
title('Depth for run 6ft 1kt')
xlabel('Time (Seconds')
ylabel('Depth(Feet)')
grid on

subplot(1,3,2)
plot(t615,r615,'b');
title('Depth for run 6ft 1.5kt')
xlabel('Time (Seconds)')
ylabel('Depth(Feet)')
grid on

subplot(1,3,3)
plot(t62,r62,'b',t62a,r62a,'r');
title('Depth for run 6ft 2kt')
xlabel('Time (Seconds)')
ylabel('Depth(Feet)')
grid on

figure(4)
subplot(1,3,1)
plot(t41,r41,'b',t41a,r41a,'r');
title('Depth for run 4ft 1kt')
xlabel('Time (Seconds)')
ylabel('Depth(Feet)')
grid on

subplot(1,3,2)
plot(t415,r415,'b',t415a,r415a,'r');
title('Depth for run 4ft 1.5kt')
xlabel('Time (Seconds)')
ylabel('Depth(Feet)')
grid on

subplot(1,3,3)
plot(t42,r42,'b',t42a,r42a,'r');
title('Depth for run 4ft 2kt')
xlabel('Time (Seconds)')
ylabel('Depth(Feet)')
grid on

%% Correlations Experimental
```

```
len=[4;6;8];
c1=[.1234; .2805; .352];
c15=[.489; .952; 1.3115];
c2=[1.037; 1.996; 2.557];

figure(5)
plot(len,c1,'b',len,c15,'r',len,c2,'m')
title('Height change vs. Length at Different Speeds')
xlabel('Approx Lengths (ft)')
ylabel('Height change (ft)')
legend('1 kt (1.69 ft/s)','1.5 kt (2.53 ft/s)','2 kt (3.38
ft/s)','Location','NorthWest')
% axis([0 8 0 3])
grid on

a1=[14.27; 17.59; 17.06];
a15=[28.63; 32.72; 33.27];
a2=[42.2; 48.14; 47.13];

figure(6)
plot(len,a1,'b',len,a15,'r',len,a2,'m')
title('Tow Angle vs. Length at Different Speeds')
xlabel('Approx Lengths (ft)')
ylabel('Linear Tow Angle (Degrees)')
legend('1 kt (1.69 ft/s)','1.5 kt (2.53 ft/s)','2 kt (3.38
ft/s)','Location','NorthWest')
axis([4 8 0 60])
grid on

spe=[1;1.5;2];
ch4=[.1234; .489; 1.037];
ch6=[.2805; .952; 1.996];
ch8=[.352; 1.3115; 2.557];

figure(7)
plot(spe,ch4,'b',spe,ch6,'r',spe,ch8,'m')
title('Height change vs. Speeds at Different Lengths')
xlabel('Speed kts')
ylabel('Height change (ft)')
legend('4 ft','6 ft','8 ft','Location','NorthWest')
% axis([0 8 0 3])
grid on

%
an4=[14.27; 28.63; 42.20];
an6=[17.59; 32.72; 48.14];
an8=[17.06; 33.27; 47.13];

figure(8)
plot(spe,an4,'b',spe,an6,'r',spe,an8,'m')
title('Tow Angle vs. Speed at Different Lengths')
xlabel('Speed kts')
ylabel('Linear Tow Angle (Degrees)')
legend('4 ft','6 ft','8 ft','Location','NorthWest')
axis([4 8 0 60])
```

```
grid on

%% Variables
g=32.2; % [ft/s/s]
rho=62.4;% [lbf/ft^3]
Cd=1.17; % Prouty
L=[4,6,8];
M = 4.83/32.2; % [lbf]
wn = 164; % [rad/s]
k = wn^2*M; % [lbf*rad2/s2]
G = 11.31e6; % [psi]
B = 0.576*k*7*12*sqrt(rho/G);

angle(1,1)=(an4(1,1)+an6(1,1)+an8(1,1))/3;
angle(2,1)=(an4(2,1)+an6(2,1)+an8(2,1))/3;
angle(3,1)=(an4(3,1)+an6(3,1)+an8(3,1))/3;
A=0.349; % Square feet
Ax=[A*cosd(angle(1,1)) A*cosd(angle(2,1)) A*cosd(angle(3,1))];
% Ax=A*cosd(45);
v=[1.6878 2.5317 3.3756]; %ft/sec

fdrag=.5.*rho.*v.^2.*Cd.*Ax;
% fprintf('Drag Force at 1 knot is %f lbf \n\n', fdrag(1));
fprintf('Drag force at 1 kt: %.2f lbf, at 1.5 kt: %.2f lbf, at 2 kt: %.2f
lbf\n\n', fdrag(1),fdrag(2),fdrag(3));

% Solve for angle wrt velocity
v = linspace(0, 4, 100);
vol = 16.65; % [in3] (0.00964 ft3)
mg = 4.83; % [lbf]

a = 0.5*(rho*A*Cd*v.^2/(vol*rho-mg));
a1 = -sqrt(4.*a+1)/(2.*a);
a2num = -sqrt( (1./a.^2) - (1./(a.^2.*sqrt(4.*a.^2+1))) -
(4./(sqrt(4.*a.^2+1))));
a2den = sqrt(2);
a2 = a2num/a2den;
a3 = 1./(2.*a);
theta = -2*atan(a1+a2+a3)*180/pi;

% plot(v, theta)
% title('Tow Angle vs. Velocity')
% xlabel('Velocity [in/sec]')
% ylabel('Tow Angle [degrees]')
% grid on
```